2

Initial Growth Process of Carbon Nanotubes in Surface Decomposition of SiC

Takahiro Maruyama and Shigeya Naritsuka
Department of Materials Science and Engineering,
Meijo University
Japan

1. Introduction

1.1 Basic property of carbon nanotube

Carbon nanotubes (CNTs) are cylinders of graphene which is a single planar sheet of sp^2-bonded carbon atoms. From their unique structures, they exhibit several novel properties, such as high strength, high performance in electrical and thermal conductors, etc. Therefore, since the discovery by Iijima in 1991 (Iijima, 1991), CNTs have been one of the hottest topics in both physics and material science. Mainly, their structures are specified with four parameters; the number of walls, diameter, length and chirality. Dependent of the number of walls, CNTs are categorized as single-walled nantoubes (SWNTs) and multi-walled nanotubes (MWNTs) and SWNT structure can be specified uniquely with a chiral vector $\boldsymbol{C}_h = n\boldsymbol{a}_1 + m\boldsymbol{a}_2$ (n, m are integers, $0 \le |m| \le n$) defined relative to the two-dimensional graphene sheet (Saito et al., 1998). Figure 1 shows the graphene honeycomb lattice. The unit cell is spanned by the two vectors $\boldsymbol{a}_1$ and $\boldsymbol{a}_2$ and contains two carbon atoms, where the basis vectors of length $a_0 = 0.246$ nm form an angle of 60°. The chiral vector $\boldsymbol{C}_h$ can be expressed by these two vectors $\boldsymbol{a}_1$ and $\boldsymbol{a}_2$, and it corresponds to a section of the SWNT perpendicular to the nanotube axis. In Fig. 1, the chiral vector $\boldsymbol{C}_h = 6\boldsymbol{a}_1 + 3\boldsymbol{a}_2$ of an (6, 3) tube is shown. The translation vector, $\boldsymbol{T}$, which is parallel to the nanotube axis and is normal to the chiral vector $\boldsymbol{C}_h$ in the unrolled honeycomb lattice is also shown and it can be expressed in terms of the basis vectors $\boldsymbol{a}_1$ and $\boldsymbol{a}_2$ as, $\boldsymbol{T} = 4\boldsymbol{a}_1 - 5\boldsymbol{a}_2$. The electronic structure of a SWNT is determined by these two indices (n, m) and the SWNTs could be semiconductors and metals, depending on them. For example, metallic CNTs show the relation, $n - m = 3q$, with q being an integer. The diameter of a SWNT, d, is also specified with these chiral indices as,

$$d = \left(\frac{a_0}{\pi}\right)\sqrt{\left(n^2 + nm + m^2\right)} \tag{1}$$

The band gap of semiconducting SWNTs is inversely proportional to the diameter. Therefore, it is important to control and obtain SWNTs with unique chirality at will, for realization of CNT devices.

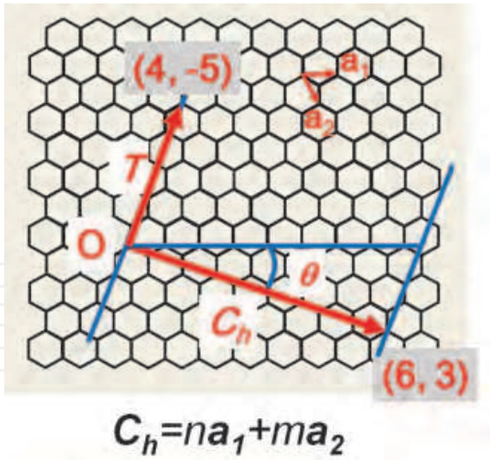

Fig. 1. Graphene honeycomb lattice with the lattice vectors a_1 and a_2. The chiral vector C_h = $6a_1 + 3a_2$ of the *(6, 3)* tube and the translation vector $T = 4a_1 - 5a$ are shown.

1.2 Carbon nanotube growth by surface decomposition of SiC

There have been three main methods to produce CNTs; arc discharge, laser ablation and chemical vapour deposition (CVD). Arc discharge and laser ablation utilize the evaporation of a graphite target to create gas-phase carbon fragments which recombine to form CNTs. Although both produce CNTs with high crystallinity due to the high growth temperature, it is difficult to control the structure of CNTs. Recently, CVD has been widely used for CNT growth because it is suitable for organizing CNTs over a large surface. CVD utilize metal catalyst particles in the gas phase or on surfaces, decomposing a carbon containing feedstock gas, such as acetylene or ethanol. These procedures can be applied to control the structure of CNTs through the size and shape of catalyst. So far, the diameters of CNTs could be controlled to some extent through the control of catalyst particle size (Jeong et al., 2007). However, there still remains some distribution in the CNT diameter, and also the control of chirality has never been achieved.

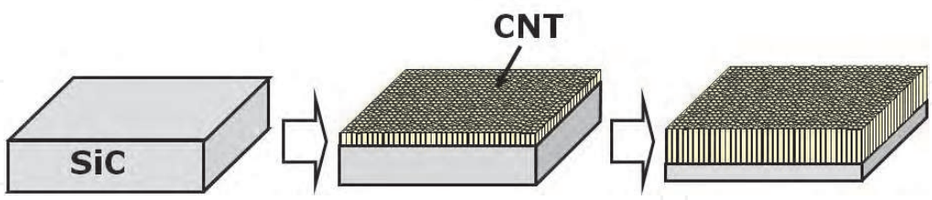

Fig. 2. Schematic illustration of CNT growth by surface decomposition of SiC.

As distinct from these conventional growth techniques, surface decomposition of SiC has been reported as a novel CNT growth technique during recent years. It was first discovered by M. Kusunoki et al. in 1997, who found that CNTs grew on SiC(-1-1-1) surface after heating a 3C-SiC single crystal at 1700°C using YAG laser during a transmission electron microscope (TEM) observation (Kusunoki et al., 1997). They observed that CNTs were mostly oriented along the [111] direction. Later, they reported that CNTs could be easily produced on 6H-SiC(000-1) surface only after heating in a vacuum electric furnace (Kusunoki et al., 2000). The schematic picture of the growth process of CNTs by surface decomposition of SiC is shown in Fig. 2. As heating temperature rises, Si atoms are desorbed

and CNTs grew into the SiC substrate the axes of which are kept perpendicular to the substrate surface. This growth method has an exclusive characteristics because it needs no catalyst, and self-aligned CNTs were grown with desorption of Si atoms.
Also, they pointed out that CNT growth was strongly dependent on the polar faces of SiC. Figures 3(a) and (b) shows schematic cross-sectional and top view of 6H-SiC, respectively, and SiC (000-1) and (0001) faces are shown at the top layer and bottom in Fig. 3(a). On the (000-1) face (carbon–face), there are dangling bonds from carbon atoms which are perpendicular to the substrate surface, while dangling bonds from Si atoms are seen on the (0001) face (Si-face). Kusunoki et al. pointed out that CNT growth was observed only on carbon-faces of SiC single crystals, such as (000-1) face of 6H-SiC and (-1-1-1) face of 3C-SiC, while graphite sheets were formed on the surface after heating Si-faces (Kusunoki et al., 2000).

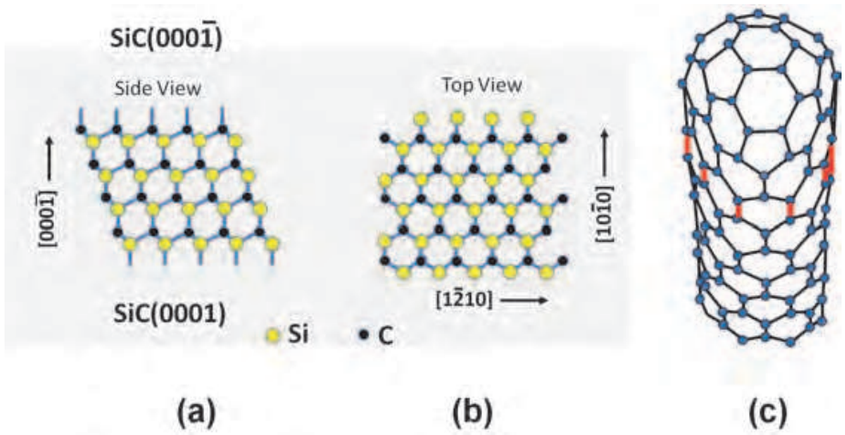

Fig. 3. Schematic representations of (a) cross-sectional view and (b) top view of 6H-SiC, and (c) zigzag-type of a SWNT. The top side and bottom side of (a) correspond to (000-1) and (0001) faces, respectively.

So far, through high-resolution TEM (HRTEM) images, they revealed several characteristics of CNTs grown by this method: (a) most CNTs are two to five layered 2-5 nm in diameter, (b) The CNTs are grown perpendicular to the SiC surface, (c) The density of CNTs is above 10^{12} cm^{-2}, which is higher than those grown by other methods, (d) The CNTs are atomically bonded with the SiC crystal at the interface and (e) most of the CNTs have unique chirality, that is, zigzag-type (Fig. 3(c)) (Kusunoki et al., 2002). Although there are still several problems to be resolved for device fabrication, such as purity of the CNT film and homogeneity in the number of walls and diameter, CNTs grown by surface decomposition of SiC have several advantages to realize CNT devices. Among these useful properties, the unique chirality of grown CNTs is the most important and mysterious, because the growth of CNTs with unique chirality has never been attained by other growth techniques. Therefore, surface decomposition method might play an important role in fabrication of CNT devices. Also, elucidation of the mechanism of selectively chirality alignment will be invaluable and useful to control and align chirality of CNTs grown with other methods.

1.3 Carbon nanocap

The formation process in the initial stage of CNT growth by surface decomposition of SiC has been reported by several groups. TEM studies by Kusunoki's group showed that arced

sheets of carbon with an outer diameter of 5 nm and height of 1-2 nm appeared on the SiC(000-1) face after heating at 1250°C for 30 min (Kusunoki et al., 2000). After heating at 1300°C, two-, to three-layered carbon nanocaps 3-5 nm in diameter and 3-5 nm in height were generated in a dense formation on the surface. After heating at higher temperature, CNTs grew below these carbon nanocaps with desorption of Si atoms indicating that these carbon nanocaps correspond to the top of CNTs. This means that the structure of CNTs is closely related to the carbon nanocaps, and elucidation of the formation mechanism of the carbon nanocaps is a key point to clarify unique chirality of CNTs grown by this method.

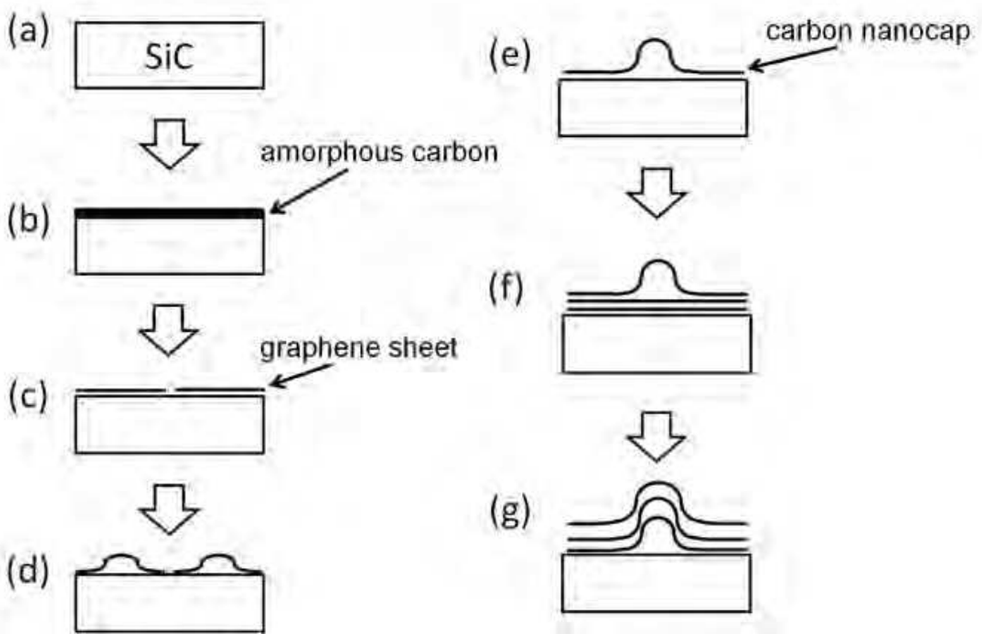

Fig. 4. Schematic illustration of the initial growth process of carbon nanocaps and CNTs proposed by Watanaebe's group.

Except for pioneering and essential investigation by Kusunoki's group, few studies have been reported about the formation mechanism of carbon nanocaps. Watanabe et al. carried out TEM and scanning tunnelling microscope (STM) observation for CNT growth on 3C-SiC(-1-1-1) and proposed a model for carbon nanocap formation. The schematic figure of their model is shown in Fig. 4 (Watanabe et al., 2001). In their model, at first, amorphous carbon was formed on the SiC surface with the evaporation of Si atoms. Then, they were crystallized and graphene flakes were formed and aligned parallel to the SiC surface with the temperature rise. Finally, lifting of part of the graphene, carbon nanocaps were formed. This model is significant as first attempt to explain this unique phenomenon. However, intuitively, their model seems to have some discrepancy against the observed experimental results; in their model, the diameter of a CNT would be enlarged, however, TEM observation showed that the diameter was maintained during the growth. Also, it seems to be difficult to explain the reason why enormously high-density CNTs are grown. To clarify the real growth process, analysis at the atomic level is essential, including the alignment and direction of C-C bonding during the crystallization

In this study, we investigated the details of formation process of carbon nanocaps using various experimental techniques; STM, X-ray photoemission (XPS) and near edge X-ray

absorption fine structure (NEXAFS) spectroscopies. Based on these experimental results, we attempted to propose a formation mechanism of carbon nanocaps.

2. Formation mechanism of carbon nanocap

2.1 Formation process of carbon nanocap

To clarify the details of formation process of carbon nanocaps, it is essential to clarify the surface structure and composition. However, few studies have been reported with combing XPS measurement and STM observation for formation process of carbon nanocaps. Here, we carried out both XPS measurements and STM observations for carbon nanocaps formed on 6H-SiC(000-1) (Maruyama et al., 2006, 2007). Figure 5(a) and (b) show XPS spectra of 6H-SiC(000-1) surface before and after heating at 1100°C in UHV, respectively, where the spectrum of Fig. 5(a) is that from the sample after etching with 10% HF for 15 min. To grow carbon nanocaps, the temperature was slowly increased, keeping the heating rate below 2°C/min in the temperature region above 400°C. Both spectra were measured at room temperature with a laboratory photon source ($Mg\ K_\alpha$: 1253.6 eV) at the take-off angle of 20° from the surface plane, to enhance the surface sensitivity. As expected, no elementary carbon was observed before heating. It should be noted that some oxides such as $Si_xC_yO_z$ are main components on the surface and the SiC component is weak. Taking into account that the escape depth of photoelectron was about only one nanometer in the measurement condition, most of SiC(000-1) surface was covered with these oxides even after HF etching. After heating at 1100°C, a component of elementary carbon derived from sp^2 bonding became dominant, corresponding to both desorption of Si. The component from the SiC substrate is still observed, which suggests that the carbon layer accumulated on the SiC surface was very thin and about a few nanometers. Relative intensity of each component in XPS spectra was estimated as the sum should be one, and its temperature dependence is shown in Fig. 5(c). After heating above 1000°C, the component of elementary carbon (sp^2) appeared and it gradually increased, as the heating temperature rose. On the other hand, those related from SiC and $Si_xC_yO_z$ gradually decreased with the temperature, although a small amount of oxides still remained at 1200°C. The increase of the component of carbon sp^2 bonding correspond to the progress in the desorption of Si atoms and the accumulation of carbon atoms on the SiC surface, which leads to carbon nanocap formation.

Surface structure change with the heating temperature is shown in Fig. 6. These STM images were observed at room temperature after heating at each temperature in UHV. After heating at 800°C, step-like structures appeared on some portion of the surface (a). The area of each terrace was small and several tens of nanometers. After heating at 1100°C, densely packed grains, around 1-2 nm in size, were observed over the entire surface (b). These nanoparticles formed clusters at 1150°C, keeping the sizes of individual particles unchanged (c). The cluster size ranged from around 3 to 5 nm. Taking into account the result of XPS measurements, the nanoparticles were elemental carbon which were accumulated after desorption of Si. After heating at 1200°C, the SiC surface was covered by a large number of grains ranging in size from around 3 to 5 nm, as shown in STM images of Fig. 6(d). The blowup in Fig. 6(d) shows that their surfaces were covered with cobweb-like patterns, indicating that the carbon nanocaps were formed at this temperature.

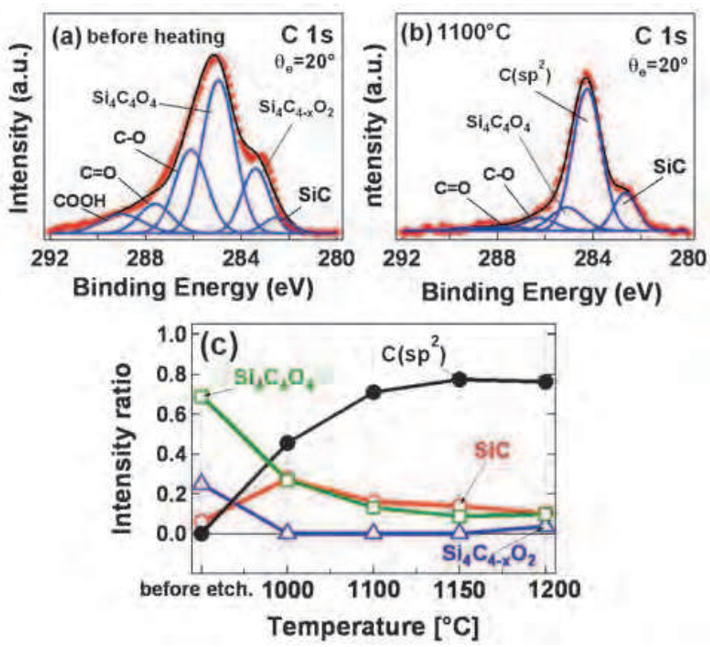

Fig. 5. XPS spectra of SiC(000-1) surface of (a) before heating (after HF etching), and (b) after heating at 1100°C in UHV. Both spectra were measured at the take-off angle of 20°from the surface plane. (c) Temperature dependence of relative intensities of each component in XPS spectra.

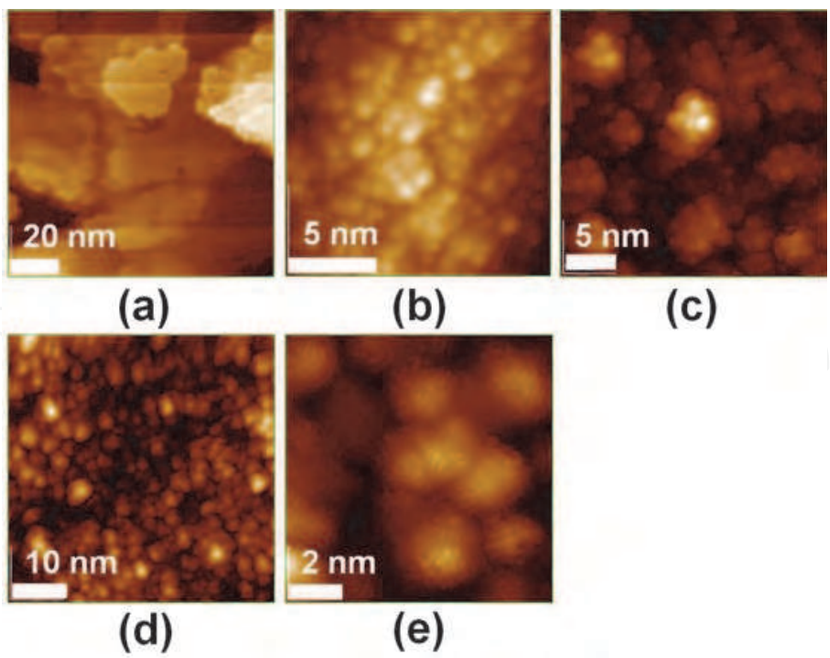

Fig. 6. STM images of 6H-SiC(000-1) substrate obtained in subsequent stages of the annealing process under UHV: (a) after annealing at 800°C, (b) 1100°C, (c) 1150°C, and (d) and (e) 1200°C. (e) is a blowup of (d).

Figure 7 shows another STM images for carbon nanocaps formed on SiC(000-1) which were annealed at 1250°C in a vacuum electric furnace (Bang et al., 2006). Carbon nanocaps formed on the entire surface were clearly shown in (a). Figure 7(b) shows an atomic-resolution STM images of the blowup of a cap structure produced on a 6H-SiC(000-1) substrate. They showed convex structures, 3-5 nm in diameter and 1-2 nm in height, exhibiting cobweb-like patterns, as shown in Fig. 6(e).

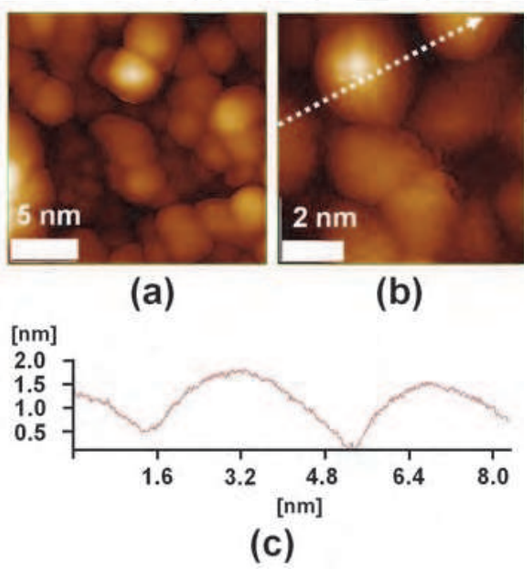

Fig. 7. (a) and (b) STM image of the cap structures produced on 6H-SiC(000-1) substrates after heating at 1250°C in a vacuum electric furnace. (c) Height profile of cap structures in the direction marked by an arrow in (b).

Figure 8(a) shows one portion of the surface of a carbon nanocap formed on 6H-SiC(000-1) after annealing in a vacuum electric furnace and (b) and (c) show magnified feature of STM images of (a). Figure (b) and (c) are the same except for the markers shown by open circles and a square. (Bang et al., 2006). Figure 8(b) clearly reveals the cobweb-like pattern, which corresponds to carbon networks, on the surface of carbon nanocaps. In Fig. 8(c), one large circle, one large square, and nine small circles can be seen. There are six small open circles around the right large open circle, which confirms that this pattern is a carbon network composed of hexagons. In contrast, the left large square is surrounded by only five small circles, which indicates that the portion of network represented by the left large open square is a pentagon on the nanocap surface. It is well known that a convex carbon network contains several pentagons, as observed on the surface of fullerenes. Given the convex shape of the nanocap, it is reasonable to observe a pentagon on the surface. These STM observations support the assumption that the carbon nanocap had been already crystallized when it was formed on the SiC surface.

Crystallization during the formation of carbon nanocaps was directly confirmed by *in situ* NEXAFS measurements. The left part of Fig. 9 shows carbon *K* edge NEXAFS spectra of SiC(000-1) surfaces at 1190 and 1250°C obtained using a synchrotron light source. All spectra were measured in Auger electron yield detection mode, with the sample maintained at the heating temperature to carry out *in situ* measurements. The arrangement of the sample and the synchrotron radiation source is shown schematically in the right part of Fig. 9, where the

angle between the incident X-rays and the electron energy analyzer was fixed at 60°, and the incident angle, θ, is defined as the angle between the light source direction and the sample surface. In Fig. 9, NEXAFS spectra obtained with different θ values are shown for each temperature and are normalized to the highest peaks. The light from the synchrotron source was linearly polarized, so that when θ = 90°, the electric field vector, E, is parallel to the sample surface, whereas when θ = 30°, E contains components both parallel and perpendicular to the surface.

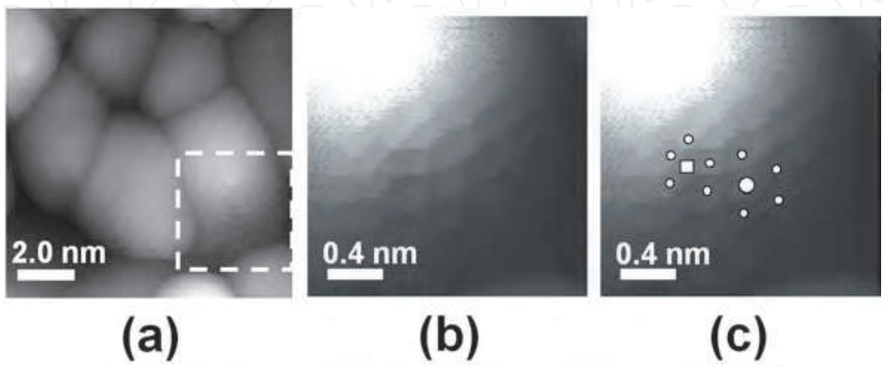

Fig. 8. (a) STM image of another region of the sample shown in Fig. 7. (b) and (c) Magnified feature of STM images of the cap structures in (a). (b) and (c) are exactly the same image, except for the open circle and square markers in (c). The large circle on the right is surrounded by six small circles, while the large square on the left is surrounded by five small circles.

As seen in Fig. 9, for both incident angles, and irrespective of the temperature, sharp C-C π* resonance peaks were observed at approximately 285 eV in all spectra. In addition, at 1250°C, broad σ* resonances were observed in the region from 290 to 315 eV, accompanied by a sharp σ* bound exciton at ~291.5 eV ((a) and (b)). These two peaks are characteristic of carbon materials composed of well-ordered graphene sheets. Therefore, the spectra in Figs. 9(a) and (b) are expected to be associated with carbon nanocaps. At 1190°C, slight differences were observed between the spectra for the two incident angles. At θ=30°, the spectrum was quite similar to that at 1250°C. On the other hand, at θ=90°, the relative intensity of the σ* to the π* resonance increased, and the σ* bound exciton peak became blurred. It has been reported that for amorphous carbon, the NEXAFS spectrum exhibits a structureless σ* resonance and the relative intensity of the σ* to the π* resonance is higher than that for graphite (Comeli et al., 1988). Therefore, the spectra at 1190°C were considered to be derived from a mixture of ordered graphene layers and amorphous carbon. Taking the STM results into account, the spectra at 1190°C are associated with crystallization during the production of carbon nanocaps. It is well known that the π* resonance peak is strongly enhanced when the electric field vector of the incident X-rays is parallel to the π* orbitals (Banerjee et al., 2005). Therefore, the increased relative intensity of the π* resonance at θ=30° indicates that the majority of π* orbitals were nearly perpendicular to the surface, that is, most C-C bonds were directed nearly parallel the surface at the beginning of carbon nanocap formation. On the other hand, the carbon nanocaps are dome-like and they consist of graphene sheets with almost the same amount parallel and perpendicular to the SiC surface (Kusunoki et al., 2000, Bang et al., 2006). That is why there was no remarkable difference in the spectra at 1250°C for the two incident angles.

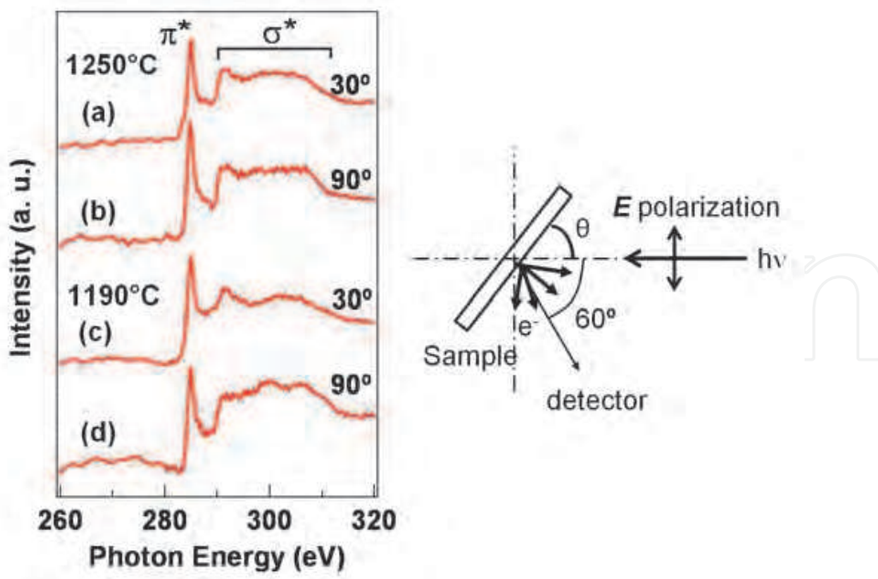

Fig. 9. Left part: NEXAFS spectra of 6H-SiC(000-1) during heating at 1250°C (a) and (b), and 1190°C(c) and (d). The spectra of (a) and (c) were measured at an incident angle of light source was 30°, while those of (b) and (d) were at 90°. Right part: Scheme of registration of angular dependence of NEXAFS, where E and θ is electric field vector and incidence angle of X-ray beam. The incidence angle, θ, is measured as an angle between the direction of X-ray and the sample surface and the angle between the incident X-ray and the electron energy analyzer was fixed at 60°.

2.2 Mechanism of chirality alignment to zigzag-type

One of the most significant and important characteristics of CNT films grown by surface decomposition of SiC is their unique chirality. As stated above, Kusunoki et al. pointed out that the CNTs mostly exhibit zigzag-type chirality (Kusunoki et al., 2002). Taking into account that the carbon nanocaps were the tips of CNTs and that CNTs grow from below the carbon nanocaps, this suggests that they have chemical bonds perpendicular to the SiC(000-1) surfaces at its periphery, connected with zigzag-type CNTs (Fig. 3(c)). On the other hand, considering that aligned CNTs were apt to form on the carbon-face of SiC, Irle et al. pointed out that dangling bonds of carbon-face play a key role to form cap structures, based on quantum chemical molecular dynamics simulations (Irle et al., 2006).

Our XPS and STM results show that amorphous carbon nanoparticles are accumulated on SiC surface before the carbon nanocap formation (Maruyama et al., 2006). These nanoparticles assemble and coalesce as the temperature rises and finally are crystallized to carbon nanocaps. From the NEXAFS results, majority of C-C bonds are directed toward perpendicular to the surface at the beginning of crystallization. Therefore, utilizing dangling bonds on SiC surface, crystallization occurred, which serves to form carbon nanocaps. Considering that the final structure is a dome-like, the bond alignment perpendicular to the surface should occur circumferentially.

On the basis of the various experimental results, we propose a model for carbon nanocap formation by surface decomposition of SiC. Schematic images are shown in Fig. 10. (1) At first, carbon nanoparticles are accumulated as Si atoms are desorbed from SiC surface. (~1100°C) (2) Upon heating, carbon particles start migration on the SiC surface as a result of

the thermal energy, forming clusters of several tens of carbon nanoparticles to reduce the surface energy further (~1150ºC) (Fig. 10(b)). Then, the redistribution of carbon atoms begins within each nanoparticle cluster, and the nanoparticles begin to coalesce (Fig. 10(c)). At around 1200ºC, coalescence proceeds within the clusters, and crystallization occurs, forming CNT nanocaps. In the crystallization, the size of clusters is presumably almost the same as that of the formed nanocaps. Thus, we believe that the size of clusters determines the nanocap size. (5) Above 1200ºC, CNT growth into SiC proceeds by the sublimation of Si atoms from the SiC(000-1) surface. The NEXAFS spectra which suggest that the C-C bonds are directed nearly parallel to the surface at the beginning of crystallization, indicates that the direction of C-C bonds were changed during the crystallization. (Some difference might be seen in the measurement temperature between STM and NEXAFS because of the detection limitation of a pyrometer.) Taking into account the final structure of carbon nanocaps, we speculate that crystallization occurs at the periphery of amorphous carbon dome, and formation of C-C bonding utilize the dangling bonds from carbon atoms on the SiC(000-1) surface (Fig. 10). From the standpoint of crystal growth, this means that nucleation starts to occur at the edge in the carbon nanocaps.

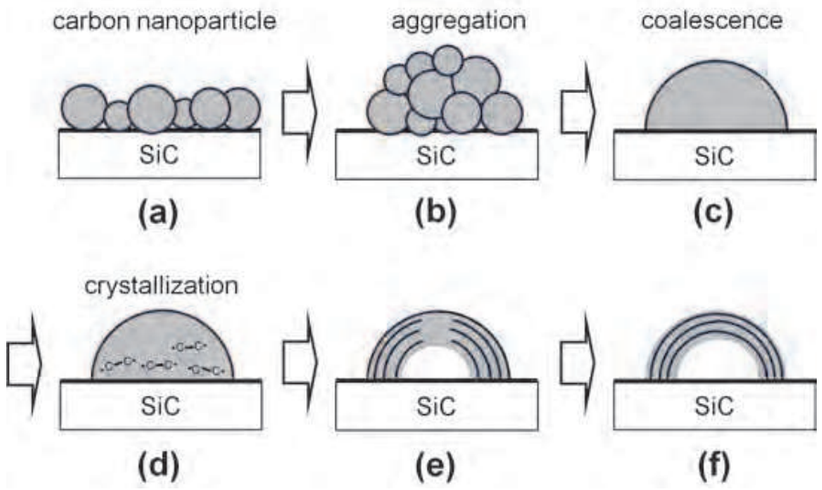

Fig. 10. Schematic model of the carbon nanocap formation process during surface decomposition of SiC. (a) formation of carbon nanoparticles by surface decomposition of SiC, (b) aggregation of carbon nanoparticles, (c) coalescence, (d) start of crystallization utilizing the dangling bonds, (e) progress of crystallization, and (f) complete formation of carbon nanocap. (The portion consisting of elementary carbon is shown as grey area.)

Recently, graphene growth from SiC(000-1) carbon-face by surface decomposition has been reported and a lot of researchers have been focusing on it because of its superiority in electronic property (Jernigan et al., 2009, Tedesco et al., 2009). From the point of view of growth technique, the method of graphene growth on SiC(000-1) is remarkably similar to that of CNT growth by surface decomposition, but one significant difference is the heating rate. In the growth of graphene, in general, the temperature of SiC is quickly increased to the growth temperature, typically, about several minutes to ~1400ºC (Gamara et al., 2008). On the other hand, in the CNT growth by surface decomposition, the heating rate is typically 1-15ºC/min (Kusunoki et al. 1999, 2002) and much slower than that in the graphene growth. This low heating rate might be necessary to enhance the migration of carbon atoms, assembling and leading to formation of carbon nanocaps.

3. Effect of ambient oxygen gas

In early studies, Kusunoki et al. proposed a chemical reaction process for CNT growth by surface decomposition of SiC as follows (Kusunoki et al. 1999):

$$SiC(s)+1/2O_2(g) \rightarrow C(s) +SiO(g) \quad (2)$$

In their CNT growth, heating of SiC was carried out using a vacuum electric furnace whose pressure was about 10^{-2} Pa. In this circumstance, residual gases, such as O_2, H_2O, CO etc., should exist in the furnace during the growth. They considered that these residual gases reacted with Si atoms on SiC surface, leading to the desorption.
Fig. 11. shows C 1s XPS spectra for 6H-SiC at 1270°C under various oxygen pressures. The main peak at around 284.3 eV and the shoulder peak at around 282.7 eV are derived from carbon sp^2 and SiC components, respectively, and these spectra are normalized with the main peaks. It is clearly shown that the ratio of the peak intensity of the SiC component to that of the carbon sp^2 component decreased as the oxygen partial pressure increased, confirming that oxygen enhances the decomposition of the SiC surface and promoting the carbon nanocap formation. Thus, surface reaction represented with eq. (2) seems to be reasonable. In the case of CNT growth in a vacuum electric furnace, the main reaction may be replaced by the reactions as follows, since residual gases are mainly composed of CO and H_2O.

$$SiC(s)+CO(g) \rightarrow 2C(s) +SiO(g) \quad (3)$$

or

$$SiC(s)+H_2O(g) \rightarrow C(s)+ SiO(g)+ H_2(g) \quad (4)$$

As for the reaction of oxygen with SiC surface, thermal oxidation of SiC surface has been an interesting theme from a fundamental surface science perspective, since it is chemically much more complex than that of Si. So far, three distinct regions have been observed in the phase diagram describing the SiC+O_2 interaction; "passive oxidation", "active oxidation" and "surface segregation of carbon" (Song & Smith, 2002). In the passive oxidation, which occurs under high oxygen pressure and low temperature, SiO_2 layer grows on the surface, and, in the active oxidation, which occurs under low oxygen pressure and high temperature, SiC surface is etched by the reaction with oxygen. In addition, under the lower oxygen pressure and the higher temperature, surface segregation of carbon has been observed. The CNT growth by surface decomposition of SiC should occur under the third mode where segregation of carbon atoms proceeds on the surface. However, it has not been well investigated between the reaction with oxygen gas and the CNT growth in surface decomposition of SiC. To clarify these, it is necessary to minutely control oxygen pressure and investigate the relation among the pressure, temperature and surface decomposition of SiC during the CNT growth.
Fig. 12 shows a phase diagram for the interaction of O_2 with the SiC surface, where formation of carbon nanocaps and SiO_2 are separately shown (Maruyama et al., 2007). All data were obtained by heating the 6H-SiC(000-1) in a vacuum electronic furnace and in a UHV chamber where the oxygen gas was introduced by controlling the pressure, and the heating rates were kept below 1°C/min which were low enough to form carbon nanocaps. In the figure, the surface covered with carbon nanocaps, elemental carbon (not formed nanocaps), SiO_2, and tiny amount of SiO_2 (weak SiO_2 peak was observed in XPS spectra) are

shown as open circles, open squares, solid squares and solid triangles, respectively. In addition, the boundary between passive oxidation (P. O.) and active oxidation (A. O.) and that between active oxidation (A. O.) and "surface segregation of carbon (S. C) " which were obtained by extrapolating the experimental results for thermal oxidation of 6H-SiC(000-1) reported by Song and Smith (Song & Smith 2002) to wider ranges in both oxygen pressure and temperature. In their data, the critical oxygen pressure at which the active-transition occurred was estimated to be,

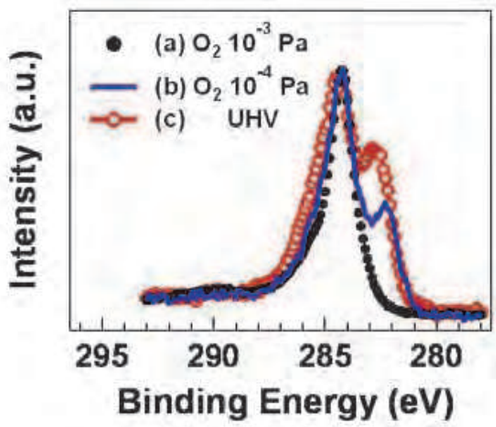

Fig. 11. C 1s XPS spectra for 6H-SiC(000-1) after heating at 1270°C for 30 min under UHV and various oxygen partial pressures (10^{-4} and 10^{-3} Pa).

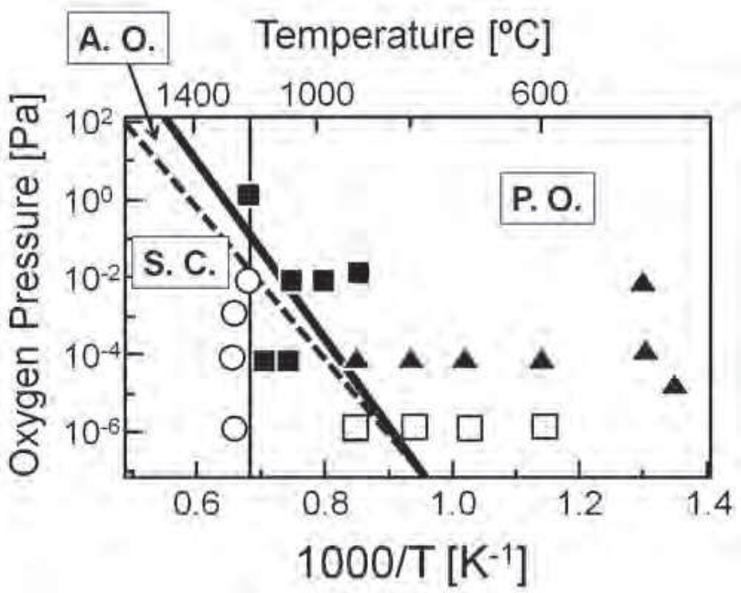

Fig. 12. Phase diagram for the interaction of O_2 with the 6H-SiC(000-1) face. Our experimental results are indicated: the open circles, open squares, solid squares and solid triangles correspond to the surfaces covered with carbon nanocaps, elemental carbon (not formed nanocaps), SiO_2, and tiny amount of SiO_2. The active-passive oxidation (A. O. –P. O.) and active oxidation (A. O.) - "surface segregation of carbon" (S. C.) boundaries reported by Ref. (Song and Smith, 2002) are also shown as thick solid line and dashed line, respectively.

$$P_c(O_2, T) = P_0 \exp(-\Delta E / k_B T) \quad (5)$$

where $P_0 = 2.7 \times 10^{15}$ *Pa* and $\Delta E = 4.8$ *eV*. It should be noted that carbon nanocaps were formed in the "surface segregation of carbon" region, and formation of carbon nanocap was observed above 1200°C, irrespective of the ambient pressure. This indicates that the heating above 1200°C is necessary to coalesce and crystallize amorphous carbon layer to form nanocaps.

Previous studies reported that graphitization of amorphous carbon occurs just above 1000°C (Botti, 2005; Chadderton & Chen, 1999). In the case of CNT growth by surface decomposition of SiC, both accumulation of sufficient carbon atoms and carbon migration are important to form carbon nanocap. This might lead to necessity of the higher temperature. On the other hand, SiO_2 layers were formed on the SiC surface in the passive oxidation region, except for the UHV region, where slight elementary carbon was seen because of insufficient oxygen gas. Although, in our experimental result, data were not obtained in the just active oxidation region, shown between the dashed line and solid line, it was clearly shown that carbon nanocaps were formed above 1200°C in the "surface segregation of carbon" region.

4. Effect of ambient hydrogen gas

Effect of hydrogen gas on carbon nanocap and CNT formation is another interesting theme, since reduction of residual oxides on SiC surfaces has been reported after annealing SiC in ambient hydrogen gases (Seyller, 2004) and this may affect the formation of carbon nanocaps. Figure 13 shows survey XPS spectra for SiC(000-1) surfaces after annealing at 1250°C for 30 min in a hydrogen atmosphere at various pressures (Ueda et al., 2010). The O 1s peak was not observed for the samples annealed at 10^{-3} and 10^{-2} Pa, whereas the O 1s peak was clearly observed for that annealed at 10^{-4} Pa. Figures 14(a) and (b) shows Si 2p and C 1s spectra for 6H-SiC(000-1) after annealing at 1250°C in a hydrogen atmosphere of 10^{-2} Pa.

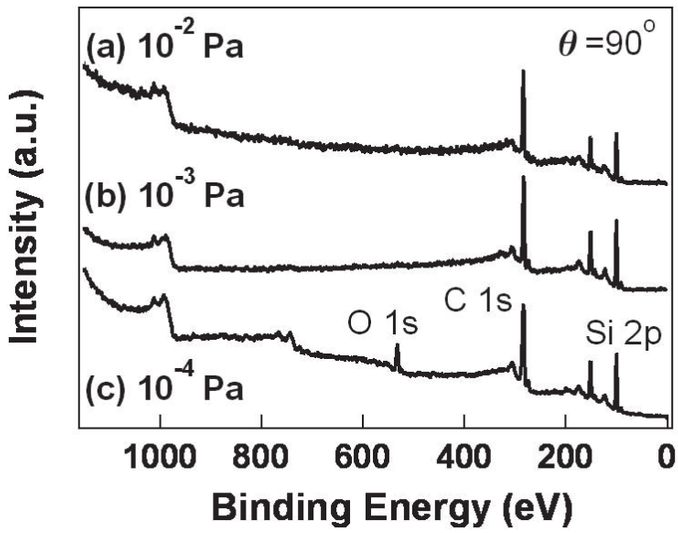

Fig. 13. XPS survey spectra for 6H-SiC(000-1) substrates after annealing at 1250°C in a hydrogen atmosphere of: (a) 10^{-2}, (b) 10^{-3} and (c) 10^{-4} Pa.

For comparison, Si 2p spectrum of the sample after annealing at 1250°C in a UHV is also shown in (c). In the Si 2p spectrum for the sample after annealing in a hydrogen atmosphere, only SiC component was observed and the component of $Si_xC_yO_z$ related oxides were negligible, while there still remain some oxides after annealing in a UHV. These results confirm removal of residual $Si_xC_yO_z$ oxides by annealing a hydrogen atmosphere of sufficient high pressure, as reported by Seyller. Figure 14(b) shows a C 1s XPS spectrum of the same sample. Except for a peak derived from adsorbed CO molecules, the spectrum consists of only a SiC-component at 282.7 eV and carbon sp^2 hybridization bonding at 284.3 eV, and no $Si_xC_yO_z$ related oxides components were observed, consistent with the Si 2p spectrum in (a).

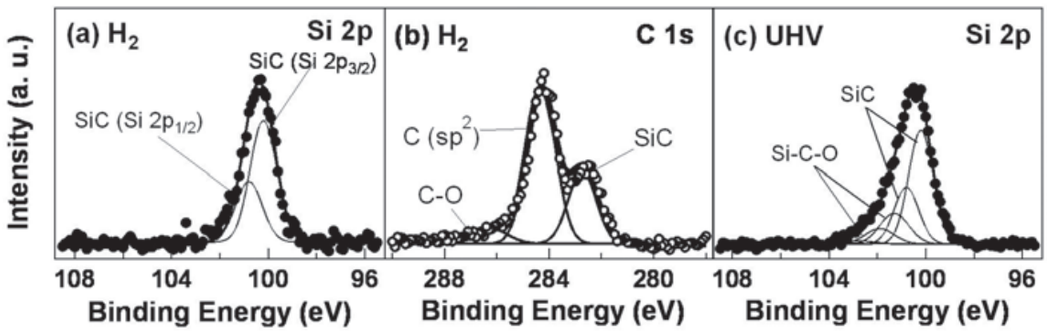

Fig. 14. (a) Si 2p and (b) C 1s XPS spectra for 6H-SiC(000-1) substrates after annealing at 1250°C in a hydrogen atmosphere of 10^{-2} Pa. (c) Si 2p XPS spectrum for 6H-SiC(000-1) substrates after annealing in a UHV. All spectra were deconvoluted into a set of Gaussian peaks after implementing background subtraction that accounted for previous XPS spectra of SiC (Hornetz et al., 1995).

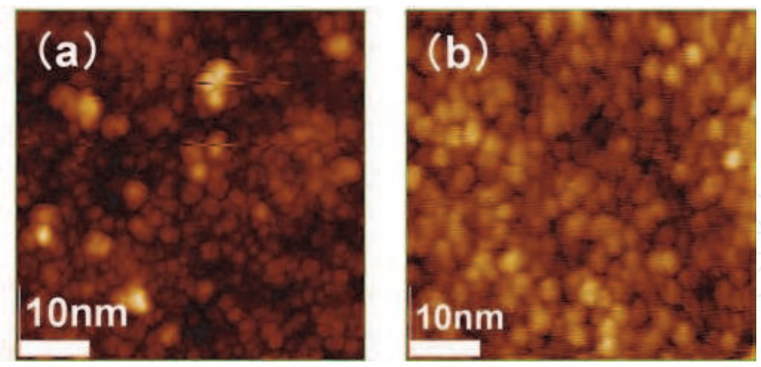

Fig. 15. STM images of 6H-SiC(000-1) for 30 min after annealing at 1200°C in (a) a UHV and (b) a hydrogen atmosphere of 10^{-2} Pa.

STM images of SiC(000-1) substrates after annealing at 1200°C for 30 min in the UHV and a hydrogen atmosphere of 10^{-2} Pa are shown in Fig. 15 (Ueda et al., 2010). The images reveal that convexities corresponding to carbon nanocaps were presented over the entire surface, independent of the annealing conditions. On the sample surface annealed in a UHV, the resulting carbon nanocaps were mainly in the diameter range of 1-3 nm, but nanocaps of more than 4 nm were observed. There were also some areas where no carbon nanocaps were

formed. On the other hand, carbon nanocaps whose diameters were mainly distributed between 3 and 4 nm were formed on the SiC surface annealed in a hydrogen atmosphere, as shown in Fig. 15(b). The change in the diameter distribution is summarized in Fig. 16, which shows histograms of carbon nanocap diameter after annealing in a hydrogen atmosphere of 10^{-2} Pa. They indicates that the distribution of carbon nanocap diameter after annealing in the hydrogen atmosphere was narrower than that found in the UHV, demonstrating that the homogeneity of carbon nanocaps can be improved by reducing the native oxide from the SiC(000-1) surface.

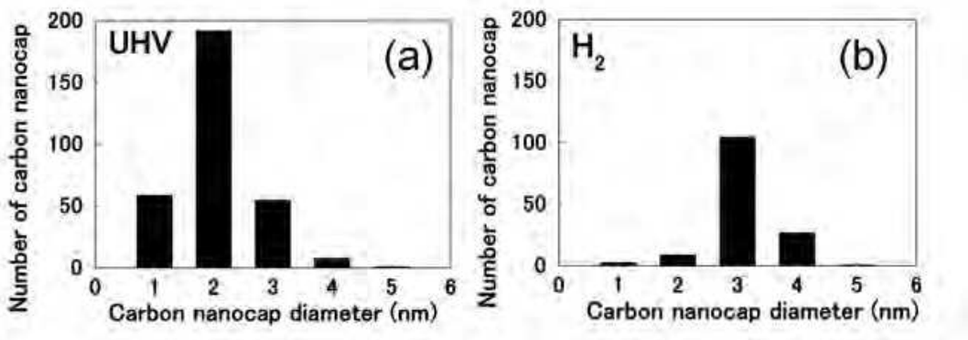

Fig. 16. Histograms, (a) and (b), of carbon nanocap diameter correspond to the samples shown in Fig. 15(a) and (b), respectively.

XPS result suggests that native $Si_xC_yO_z$ oxide on 6H-SiC still remain even after carbon nanocap formation without pre-annealing in H_2 ambient (Fig. 5(b)). Therefore, carbon nanocap formation should be disturbed among the areas covered with the oxides, because those areas should be suppressed sublimation of Si atoms. Such a localized suppression will induce an inhomogeneous distribution of an amorphous carbon layer, which, in turn, will have a deleterious effect on the size uniformity of the resulting carbon nanocaps. On the other hand, if there is no native oxide on the surface, simultaneous desorption of Si atoms would occur and homogeneous distribution of amorphous carbon layer would be formed. This process would produce carbon nanocaps with a uniform size.

5. Conclusion

CNT growth by surface decomposition of SiC is not only an interesting method as peculiar crystal growth but also has various characteristics useful for device applications. Development of this growth technique should directly lead to realization of CNT devices in future, replaced by conventional semiconductor devices. There still remain several problems to be solved for fabrication of CNT devices. To understand its growth mechanism is essential to control structural parameters of CNTs, which is absolutely necessary for realization of CNT devices. To clarify the formation process of carbon nanocaps, which are precursors of CNTs, determining the structures of CNTs, is the first step to reach this objective.

6. Acknowledgment

The authors are grateful to Prof. Amemiya for his help during NEXAFS measurements and also thank Dr. Ito, Mr. Kawamura, Ms. Fujita and Mr. Tanioku for assisting with our study

on STM observation. A part of this work was supported by the Japan Society for the Promotion of Science (JSPS), a Grant-in-Aid for Scientific Research (C) 17560015 and 21510119, and by the Ministry of Education, Culture, Sports, Science and Technology (MEXT) through the 21st century COE program "Nano Factory". We are grateful to Professor T. Yokoyama and Dr. T. Nakagawa of the Institute for Molecular Science (IMS), Okazaki, for providing the XPS facility through the Nanotechnology Support Project in Central Japan, financially supported by the Nanotechnology Network. The NEXAFS measurements were performed under the approval of Photon Factory Program Advisory Committee (Proposal No. 2009G530). We would also like to to thank the Academic Research Institute of Meijo University for their financial support.

7. References

Banerjee, S., Hemrj-Benny, T., Sambasivan, S., Fisher, D. A., Misewich, J. A. & Wong, S. S. (2005). Near-Edge X-ray Absorption Fine Structure Investigations of Order in Carbon Nanotube-Based Systems, *The Journal of Physical Chemistry B*, Vol. 109, No. 17, (October 2004), pp. 8489-8495, ISSN 1520-6106.

Bang, H., Ito, Y., Kawamura, Y., Hosoda, E., Yoshida, C., Maruyama, T., Naritsuka, S. & Kusunoki, M. (2006). Observation of Nanosized cap Structurese on 6H-SiC(000-1) Substrates by Ultrahigh-Vacuum Scanning Tunneling Microscoy, *Japanese Journal of Applied Physics*, Vol.45, No.1A, (January 2006), pp.372-374, ISSN 0021-4922.

Botti, S. Ciardi, R., Fabbri, F., Larciprete, R., Goldoni, A., Gregoratti, L., Kaulich, B. & Kiskinova, M. (2005). Electron microscopy and photoelectron spectromicroscopy study of catalyst-free transformation of carobn nanoparticles into nanotubes, *Journal of Applied Physics*, Vo.98, No.8, (October 2005), pp.084307-1-084307-6, ISSN 0021-8979.

Camara, N., Rius, G., Huntzinger, J. –R., Tiberj, A., Magaud, L., Mestres, N., Godignon, P. & Camassel, J. (2008). Early stage formation of graphene on the C face of 6H-SiC, *Applied Physics Letters*, Vol.93, No.26, (December 2008), pp.263102-1-263102-3, ISSN 0003-6951.

Chadderton, L. T. & Chen, Y. (1999). Nanotube growth by surface diffusion, *Physcis Letters A*, Vol.263, No.4-6, (December 1999), pp.401-405, ISSN 0375-9601.

Comelli, G., Stohr, J., Robinson, C. J. & Jark, W. (1988). Structural studies of argon-sputtered amorphous carbon films by means of extended x-ray-absorption fine structure, *Physical Review B*, Vol. 38, No. 11, (October 1988), pp. 7511-7519, ISSN 1098-0121.

Hornetz, B., Michel, H.-J. & Halbritter, J. (1995). Oxidation and 6H-SiC-SiO_2 interfaces, *J. Vac. Sci. Technol. A* Vol. 13, No. 3, (June 1995), pp. 767-771, ISSN 0734-2101.

Iijima, S. (1991). Helical microtubules of graphitic carbon, *Nature,* Vol.354, No.6348, (November 1991) pp.56-58, ISSN 0028-0836.

Irle, S., Wang, Z., Zheng, G. & Morokuma, K. (2006). Theory and experiment agree : Single-walled carbon nanotube caps grow catalyst-free with chirality preference on a SiC surface, *The Journal of Chemical Physics*, Vol.125, No.4 (July 2006), pp.044702-1-044702-4, ISSN 0021-9606.

Jeong, G. H., Suzuki, S., Kobayashi, Y., Yamazaki, A., Yoshimura H. & Homma, Y. (2007). Size control of catalytic annoparticles by thermal treatmnet and its application to

diameter control of single-walled carbon nanotube, *Applied Physcs Letters,* Vol.90, No.4, (Janualy 2007), pp.043108-1-043108-3, ISSN 0003-6951.

Jernigan, G. G., VanMil, B. L., Tedesco, J. L., Tischler, J. G., Glaser, E. R., Davidson, III, A., Cambell, P. M., & Gaskill, D. K. (2007). Comparison of Epitaxial Graphene on Si-face and C-face 4H SiC Formed by Ultrahigh Vacuum and RF Furnace Production, *Nano Letters*, Vol.9, No.7, (September 2009), pp.2605-2609, ISSN 1530-6984.

Kusunoki, M., Rokkaku, M. & Suzuki, T. (1997). Epitaxial carbon nanotube film self-organizaed by sublimation decomposition of silicon carbide, *Applied Physics Letters*, Vol.71, No.18, (September 1997), pp.2620-2622, ISSN 0003-6951.

Kusunoki, M., Suzuki, T., Kaneko, K. & Ito, M. (1999). Formation of self-aligned carbon nanotubes films by surface decomposition of silicon carbide, *Philosophical Magazine Letters*, Vo.79, No.4, (April 1999), pp.153-161, ISSN 0950-0839.

Kusunoki, M., Suzuki, T., Hirayama, T. & Shibata, N. (2000). A formation mechanism of carbon nanotube films on SiC(0001), *Applied Physics Letters*, Vol.77, No.4, (July 2000), pp.531-533, ISSN 0003-6951.

Kusunoki, M., Suzuki, C. Honjo, T., Hirayama, T. & Shibata, N. (2002). Selective synthesis of zigzag-type aligned carbon nanotubes on SiC(000-1) wafers, *Chemical Physics Letters*, Vol.366, No.5-6, (December 2002), pp.458-462, ISSN 0009-2614.

Maruyama, T., Bang, H., Kawamura, Y., Fujita, N., Tanioku, K., Shiraiwa, T., Hozumi, Y., Naritsuka, S. & Kusunoki, M. (2006). Scanning-tunneling-microscopy of the formation of catobn nanocaps on SiC(000-1), *Chemical Physics Letters*, Vol.423, No.4-6, (June 2006), pp.317-320, ISSN 0009-2614.

Maruyama, T., Bang, H., Fujita, N., Kawamura, Y., Naritsuka, S. & Kusunoki, M. (2007). STM and XPS studies of early stages of carbon nanotube growth by surface decomposition of 6H-SiC(000-1) under various oxygen pressures, *Diamond & Related Materials,* Vol.16, No.4-7, (January 2007), pp.1078-1081, ISSN 0925-9635.

Saito, R., Dresselhaus, G. & Dresselhaus, M. S. (1998). Structure of a Single-Wall Carbon Nanotube, In : *Physical Properties of Carbon Nanotubes*, pp. 35-58, Imperial College Press, ISBN 1-86094-223-7, London.

Seyller, T. (2004). Passivation of hexagonal SiC surfaces by hydrogen termination, *Journal of Physics : Condensed Matter*, Vo.16, No. 17 (May 2004), pp.S1755-S1782, ISBN 0953-8984.

Song, Y. & Smith, F. W. (2002). Phase diagram for the interaction of oxygen with SiC, *Applied Physics Letters*, Vol.81, No.16, (October 2002) pp.3061-3063, ISSN 0003-6951.

Tedesco, J. L., VanMil, B. L., Myers-Ward, R. L., McCrate, J. M., Kitt, S. A., Campbell, P. M., Jernigan, G. G., Culbertson, J. C., Eddy, Jr., C. R. & Gaskill, D. K. (2009). Hall effect mobility of epitaxial graphene grown on silicon carbide, *Applied Physics Letters*, Vol.95, No.12, (September 2009), pp.122102-1-122102-3, ISSN 0003-6951.

Ueda, K., Iijima, Y., Maruyama, T. & Naritsuka, S. (2010). Effect of Annealing in Hydrogen Atomosphere on Carbon Nanocap Formation in Surface Decomposition of 6H-

SiC(000-1), *Journal of Nanoscience and Nanotechnology*, Vol.10, No.6, (June 2010), pp.4054-4059, ISSN 1550-7033.

Watanabe, H., Hisada, Y., Mukainakano, S., & Tanaka, N. (2001). *In situ* observation of the initial growth process of carbon nanotubes by time-resolved high resolution transmission electron microscopy, *Journal of Microscopy*, Vol.203, No.1, (July 2001) pp.40-46, ISSN 1365-2818.

Carbon Nanotubes - Synthesis, Characterization, Applications

Edited by Dr. Siva Yellampalli

ISBN 978-953-307-497-9
Hard cover, 514 pages
Publisher InTech
Published online 20, July, 2011
Published in print edition July, 2011

Carbon nanotubes are one of the most intriguing new materials with extraordinary properties being discovered in the last decade. The unique structure of carbon nanotubes provides nanotubes with extraordinary mechanical and electrical properties. The outstanding properties that these materials possess have opened new interesting researches areas in nanoscience and nanotechnology. Although nanotubes are very promising in a wide variety of fields, application of individual nanotubes for large scale production has been limited. The main roadblocks, which hinder its use, are limited understanding of its synthesis and electrical properties which lead to difficulty in structure control, existence of impurities, and poor processability. This book makes an attempt to provide indepth study and analysis of various synthesis methods, processing techniques and characterization of carbon nanotubes that will lead to the increased applications of carbon nanotubes.

INTECH
open science | open minds

InTech Europe
University Campus STeP Ri
Slavka Krautzeka 83/A
51000 Rijeka, Croatia
Phone: +385 (51) 770 447
Fax: +385 (51) 686 166
www.intechopen.com

InTech China
Unit 405, Office Block, Hotel Equatorial Shanghai
No.65, Yan An Road (West), Shanghai, 200040, China
中国上海市延安西路65号上海国际贵都大饭店办公楼405单元
Phone: +86-21-62489820
Fax: +86-21-62489821

IntechOpen